How to cite: Angew. Chem. Int. Ed. 2024, e202403432
doi.org/10.1002/anie.202403432

Lithium Oxygen Batteries

Stable Lithium Oxygen Batteries Enabled by Solvent-diluent Interaction in N,N-dimethylacetamide-based Electrolytes

Dong-Yue Yang[+], Jia-Yi Du[+], Yue Yu[+], Ying-Qi Fan, Gang Huang, Xin-Bo Zhang, and Hong-Jie Zhang**

Abstract: In the pursuit of next-generation ultrahigh-energy-density Li–O_2 batteries, it is imperative to develop an electrolyte with stability against the strong oxidation environments. N,N-dimethylacetamide (DMA) is a recognized solvent known for its robust resistance to the highly reactive reduced oxygen species, yet its application in Li–O_2 batteries has been constrained due to its poor compatibility with the Li metal anode. In this study, a rationally selected hydrofluoroether diluent, methyl nonafluorobutyl ether (M3), has been introduced into the DMA-based electrolyte to construct a localized high concentration electrolyte. The stable –CH_3 and C–F bonds within the M3 structure could not only augment the fundamental properties of the electrolyte but also fortify its resilience against attacks from O_2^- and $^1O_2$. Additionally, the strong electron-withdrawing groups (–F) presented in the M3 diluent could facilitate coordination with the electron-donating groups (–CH_3) in the DMA solvent. This intermolecular interaction promotes more alignments of Li^+-anions with a small amount of M3 addition, leading to the construction of an anion-derived inorganic-rich SEI that enhances the stability of the Li anode. As a result, the Li–O_2 batteries with the DMA/M3 electrolyte exhibit superior cycling performance at both 30 °C (359th) and −10 °C (120th).

[*] D.-Y. Yang,[+] J.-Y. Du,[+] Y.-Q. Fan, Prof. G. Huang, Prof. X.-B. Zhang, Prof. H.-J. Zhang
State Key Laboratory of Rare Earth Resource Utilization
Changchun Institute of Applied Chemistry, Chinese Academy of Sciences
Changchun, 130022, China.
E-mail: xbzhang@ciac.ac.cn
hongjie@ciac.ac.cn

D.-Y. Yang,[+] J.-Y. Du,[+] Y.-Q. Fan, Prof. G. Huang, Prof. X.-B. Zhang, Prof. H.-J. Zhang
School of Applied Chemistry and Engineering
University of Science and Technology of China
Hefei 230026, China.

Y. Yu[+]
Department of Chemistry and Waterloo Institute for Nanotechnology
University of Waterloo
200 University Ave. W., Waterloo, Ontario N2 L 3G1, Canada.

[+] These authors contributed equally to this work.

Introduction

In order to address the burgeoning energy requirements of portable devices, electric vehicles, and large-scale energy stations, it is urgent to develop a new high-capacity battery system that surpasses the ultimate energy density of commercial lithium-ion batteries.[1] Lithium oxygen (Li–O_2) batteries, boasting an ultrahigh theoretical energy density of 3500 Wh kg^{-1}, are emerging as an encouraging contender for the next-generation rechargeable batteries.[2] It is well-known that the electrolyte serves as the "blood" of the battery, which plays a pivotal role in determining the electrochemical performance.[3] Thus, the establishment of a stable electrolyte is the basis for achieving high-performance Li–O_2 batteries. However, at present, virtually all electrolytes exhibit instability against the oxygen reduction intermediates (O_2^-) generated during the discharge and charge processes.[4] For the commonly used ether and sulfone-based electrolytes in Li–O_2 batteries, O_2^- would attack the solvent molecules for α-H abstraction and oxidation reaction, respectively. This leads to electrolyte decomposition and formation of by-products to passivate the cathode, seriously impeding the practical application of Li–O_2 batteries.[5–7] Among the available solvents, N,N-dimethylacetamide (DMA) exhibits unique benefits in anti-oxidant reduction and nucleophilic stability. As shown in Figure S1a, the ^1H nuclear magnetic resonance (NMR) spectra of the DMA exhibit negligible change pre and post KO_2 treatment, indicating it could remain stable against O_2^-. However, its application in Li–O_2 batteries is significantly constrained due to the instability with the lithium metal anode.[8–10] The poor compatibility between the DMA solvent with the Li anode results in the loss of active Li and leads to the electrolyte decomposition. Additionally, uneven Li stripping/deposition could induce dendrite growth and cause battery short circuits, resulting in safety issues. Therefore, it is anticipated that ensuring the stability of the Li metal anode within the DMA-based electrolyte is expected to promote the Li–O_2 batteries to a viable technology.

High concentration electrolyte (HCE) is an effective method to protect the Li metal anode, which could reduce the number of free solvent molecules and promote the anions to participate in the Li^+ solvation sheath. Consequently, this approach weakens the reactivity between Li and electrolyte solvent to facilitate the construction of an anion-derived solid electrolyte interphase (SEI) to enhance the stability of the Li metal anode.[11,12] While increasing the electrolyte concentration could yield these benefits, it

inevitably brings about the problems of slow mass transfer and sluggish electrode kinetics caused by its high viscosity and low ionic conductivity, not to mention the high cost. Based on these issues, a localized high concentration electrolyte (LHCE) design strategy has been developed by introducing hydrofluoroether (HFE) diluents.[13] Since HFE does not have the ability to dissolve Li salts, it could facilitate the anions to involve in the Li^+ solvation structure while reducing the electrolyte concentration, maintaining the advantages inherent to HCE.[14,15] However, the commonly utilized HFE, such as 1,1,2,2-tetrafluoroethyl 2,2,3,3-tetrafluoropropyl ether (TTE) and tris(2,2,2 trifluoroethyl)orthoformate (TFEO), struggles to maintain stability in the strong oxidation environment of Li–O_2 batteries due to the abundant C–H bonds contained in their structure (Figure S2).[13,16,17] For instance, upon reaction with O_2^- and $^1O_2$, a new chemical shift appears in the ^{1}H-NMR spectra of TTE (Figure S1b, S3a), suggesting that the TTE undergoes decomposition in the presence of a strong oxidation environment. Besides, to accommodate a large amount of Li^+-anions coordination at lower electrolyte concentrations, the volume ratio of HFE to solvent typically exceeds 1:1. This would hamper the sustained operation of open Li–O_2 batteries due to the inherent volatility of HFE.[1,16] Furthermore, the difficulty in coordinating Li^+ with HFE often results in HFE predominantly executing a singular dilution function in LHCE, while neglecting the potential interaction between HFE and solvent molecules. The solvent-diluent interaction could enhance the involvement of anions in the Li^+ solvation sheath,[18] consequently forming an anion-derived SEI to safeguard the Li metal anode. Therefore, the development of an HFE that is tolerant to the strong oxidizing environments and capable of interacting with the DMA solvent molecules could potentially achieve stable and high-performance Li–O_2 batteries, thereby propelling Li–O_2 batteries to an unprecedented level.

To this end, a rationally selected HFE diluent, methyl nonafluorobutyl ether (M3), has been employed in the DMA-based Li–O_2 batteries to construct a new LHCE system (2.0 M LiTFSI-DMA/M3 (vol. 7:3)). The reduction in concentration by M3 diluent not only augments the fundamental properties of the electrolyte, but also equips it with high resilience against attacks from oxygen reduction intermediates due to the stable –CH_3 and C–F bonds in the structure. Furthermore, the strong electron-withdrawing groups (–F) presented in the M3 diluent allow it to coordinate with the electron-donating groups (–CH_3) in the DMA solvent. This coordination facilitates more Li^+-$TFSI^-$ alignments with the addition of a small amount of M3, leading to an anion-derived inorganic-rich SEI that bolsters the stability of the Li anode. The enhancement of mass transfer, electrode kinetics, and lithium anode stability through the optimization of the electrolyte leads to the development of stable and high-performance Li–O_2 batteries, which could undergo 359 cycles and 120 cycles at temperatures of 30 °C and −10 °C, respectively.

Results and Discussion

As a proof-of-concept, the cycle performance of Li||Li symmetrical cells with various concentrations of electrolyte was checked to determine the optimal Li salt concentration to stabilize the lithium metal anode in DMA-based electrolyte. As presented in Figure S4, in the 4.0 M LiTFSI-DMA electrolyte (DMA electrolyte), the battery shows much more stable discharge-charge platforms and prolonged cycle life at 0.4 mA cm^{-2}, indicating that the Li metal anode has the superior compatibility with the DMA solvents at this concentration. However, the increase in concentration inevitably results in issues such as sluggish mass transfer and electrode dynamics caused by high viscosity and low ionic conductivity. Therefore, it is necessary to introduce an HFE diluent to construct LHCE system. Regarding the selection of an HFE diluent, it is noteworthy that if the HFE molecular structure encompasses more –CH_2– and –CH– functional groups, these will inevitably decompose under the influence of oxygen reduction intermediates.[17,19] In contrast, methyl nonafluorobutyl ether (M3), characterized by its stable –CH_3 and C–F groups within its structure, could maintain stability even in the presence of O_2^- and $^1O_2$ (Scheme 1a).[6] As shown in Figure S1c and S3b, the ^{1}H-NMR spectra of the M3 solvent remain unchanged upon reaction with O_2^- and $^1O_2$, indicating the M3 solvent exhibits resistance to both the O_2^- and $^1O_2$ attacks. Furthermore, the M3 solvent is not miscible with Li salts (Figure S5) and cannot involve in the Li^+ solvation structure, meeting the fundamental criteria for serving as a diluent. In addition to the interaction between the solvent and salt, the DMA solvent molecule contains –CH_3 electron-donating groups, while the M3 molecular structure has numerous strong electron-withdrawing groups (–F). These two components are likely to draw toward each other, leading to a weak intermolecular interaction.[18] This interaction is conducive to ensure a greater number of anions participate in the Li^+ solvation sheath when the addition of a minimal amount of HFE (Scheme 1b), thereby reducing the volatility of the electrolyte. In light of the preceding considerations, a novel LHCE system, 2.0 M LiTFSI-DMA/M3 (vol. 7:3, DMA/M3 electrolyte), was prepared.

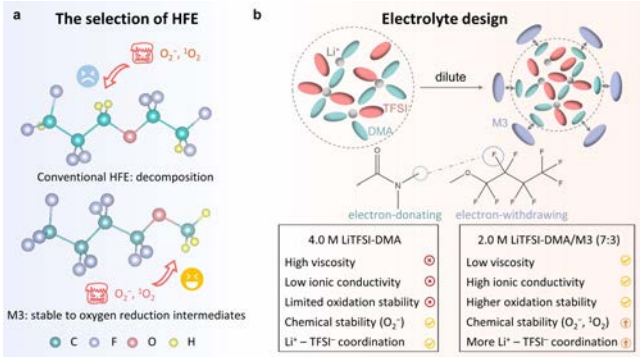

Scheme 1. (a) The selection of HFE. (b) The electrolyte design strategy.

Firstly, the properties of the high concentrated DMA electrolyte and the diluted DMA/M3 electrolyte were examined. Due to the decrease of electrolyte concentration, the DMA/M3 electrolyte has obvious optimization and improvement in terms of viscosity, ionic conductivity, and electrochemical stability window. Specifically, the DMA/M3 electrolyte exhibits a reduced viscosity of 20.4 mPa s, which is roughly one-third lower than that of the DMA electrolyte (65.1 mPa s, Figure 1a). With regard to ion transport, the ionic conductivity of the DMA/M3 electrolyte is higher than that of the DMA electrolyte at various temperatures (Figure 1b). In particular, the ionic conductivity of the DMA electrolyte (0.44 mS cm^{-1}, −20 °C) drops sharply at low temperature, while the DMA/M3 electrolyte could still maintain the ionic conductivity of 4.15 mS cm^{-1} at −20 °C, which provides a possibility for the application in low temperature Li–O_2 batteries. In addition, the DMA/M3 electrolyte displays a slightly widened electrochemical window (Figure 1c). This is attributed to the electron-withdrawing functional groups (–F) present in the M3 diluent, which improves the high voltage stability of the electrolyte.[20]

Subsequently, in order to meet the unique requirements of Li–O_2 batteries, the oxygen solubility and the stability toward the oxygen reduction intermediates were verified. As shown in Figure 1d, an incremental oxygen solubility is observed in the DMA/M3 electrolyte because of the abundant C–F groups in the M3 diluent.[17,21] Then, ^{1}H-NMR spectra were conducted to evaluate the stability of the DMA/M3 electrolyte to the O_2^- and $^1O_2$. After vigorous stirring with KO_2, no byproduct peaks are observed in the ^{1}H-NMR spectra of the DMA (Figure S6a) and DMA/M3 electrolytes (Figure 1e), indicating that both the electrolytes are stable to sustain the attack of O_2^-. In contrast, for the conventional HFE-based electrolyte, the ^{1}H-NMR spectra of the 2.0 M LiTFSI-DMA/TTE (DMA/TTE) electrolyte display a new chemical shift of 8.5 ppm after the reaction with KO_2 (Figure S6b), demonstrating that this electrolyte is decomposed with the formation of formate by-products.[22,23] For the characterization of singlet oxygen stability, $^1O_2$ was prepared by photosensitization, in which $C_{16}H_{14}$ was employed as the $^1O_2$ capture agent to prove its formation.[24] As shown in Figure 1f, two new peaks appear at the chemical shift of 7–8 ppm after $^1O_2$ treated, indicating that the $C_{16}H_{14}$ is transformed into $C_{16}H_{14}$-O_2 after illumination. It is suggested that the singlet oxygen was successfully prepared. Since the low ratio of C–H bonds in the M3 molecule, no obvious change is observed in the ^{1}H-NMR spectra before and after the generation of $^1O_2$ (Figure 1f), implying that the DMA/M3 electrolyte can defend against $^1O_2$.[17] On the contrary, formate by-products are detected in both the DMA (Figure S6c) and DMA/TTE (Figure S6d) electrolytes when exposed to the $^1O_2$. The inability of these two electrolytes to defend against the $^1O_2$ attack is attributed to the instability of the bare TTE (Figure S3a) and DMA (Figure S3c) solvents toward the $^1O_2$. Consequently, the DMA/M3 electrolyte significantly enhances interface wettability, ion transport, high voltage stability, oxygen solubility, and stability to the intermediates, laying a solid foundation for the long-term operation of Li–O_2 batteries (Figure 1g).

Based on the superior properties of the DMA/M3 electrolyte, the solvation structure of the electrolyte was further characterized by Raman and NMR spectra. The Raman spectra of the DMA/M3 electrolyte and DMA electrolytes with different salt concentrations are presented in Figure S7a. Bare DMA solvent shows bands at 732 and 953 cm^{-1}, which are assigned to the symmetric stretching $v_s(N–CH_3)$ and $v_s(C–CH_3)$ vibrations, respectively.[25] Moreover, the bands observed at 746, 1128, and 1245 cm^{-1} can be

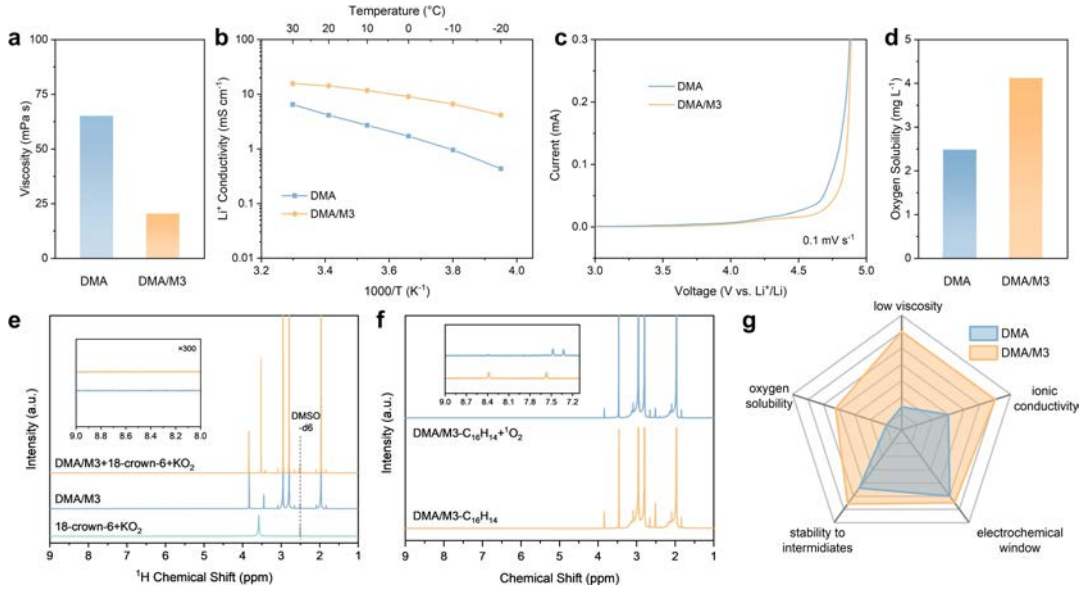

Figure 1. (a) Viscosity, (b) ionic conductivity, (c) electrochemical stability window, and (d) oxygen solubility of the DMA and DMA/M3 electrolytes. ^{1}H-NMR spectra of the DMA/M3 electrolyte toward (e) O_2^- and (f) $^1O_2$. (g) Comparison of the properties of the DMA and DMA/M3 electrolytes.

attributed to the symmetric stretching modes of SNS (v_s-(SNS)), SO_2 ($v_s(SO_2)$), and CF_3 ($v_s(CF_3)$) from $TFSI^-$, respectively.[26] As the concentration of LiTFSI salt in the bare DMA increased to 4.0 M, the peaks of free DMA solvent gradually shift toward high wavenumbers, resulting in Li^+-coordinated DMA (≈741 cm^{-1} and 961 cm^{-1}, Figure 2a, S7a). At the same time, the peak intensity of $v_s(SNS)$, $v_s(SO_2)$, and $v_s(CF_3)$ gradually increases to form Li^+-associated $TFSI^-$, indicating that the $TFSI^-$ anions gradually participate in the Li^+ solvation sheath (Figure S7b). In the case of the DMA/M3 electrolyte, both the Li^+-coordinated DMA and Li^+-associated $TFSI^-$ solvation structures are preserved (Figure 2a, S7b), suggesting that the dilution of M3 retains the properties of the 4.0 M HCE solvation structure. Subsequently, the ^{7}Li-NMR and ^{19}F-NMR spectra were employed to delve deeper into the coordination environment surrounding Li^+ in the electrolytes. The electron density around Li^+ is affected by both the anions and solvent molecules in the solvation sheath. A downfield shift with a higher ^{7}Li value is observed in the DMA/M3 electrolyte compared to the DMA electrolyte (Figure 2b), indicating the Li^+ nuclei are de-shielded due to the reduced electron cloud. This implies that the solvation of Li^+ in the DMA/M3 electrolyte is weaker compared with the DMA electrolyte. Interestingly, even in cases where the volume ratio of M3 to DMA solvent is less than 1:1, an increase in the $TFSI^-$-^{19}F signal was detected at higher fields in the DMA/M3 electrolyte, indicating an enhancement in the interaction between Li^+ and $TFSI^-$ (Figure 2c).[20] It should be noted that the ^{19}F-NMR is referenced to the $LiPF_6$ standard, with the chemical shift of 84.6 ppm and 86.1 ppm.

Given that the M3 diluent is insoluble in lithium salts, it is probable that the increased Li^+-$TFSI^-$ coordination in the DMA/M3 electrolyte results from the interaction between the DMA and M3 solvent. To elucidate the DMA-M3 solvent interaction, ^{1}H-NMR and ^{19}F-NMR spectra of the solvents were performed. As presented in Figure 2d, the ^{1}H signals of both the DMA and M3 solvents display a downfield shift toward higher values when combined in the mixed DMA/M3 solvent. Moreover, the ^{19}F signals of the M3 solvent within the DMA/M3 mixed solvent system also exhibit a downfield shift (Figure 2e, S8), indicating that the electron cloud density of F atoms in the M3 solvent is affected by the presence of the DMA solvent. These observations suggest that the existence of intermolecular interactions between the DMA and M3 solvent. This interaction could be further elucidated through the electrostatic potential (ESP) calculations (Figure S9). Within the isopotential surface of the DMA solvent, the positive charge is exclusively concentrated on the H atoms. For the M3 solvent, the more negative regions are primarily concentrated on the F atoms. The strong electron-withdrawing groups (–F) in the M3 diluent facilitate its coordination with the electron-donating groups ($–CH_3$) in the DMA solvent. Besides, the intermolecular energy of the solvents was calculated to investigate the variations in their interaction, which was precisely adjusted for basis set superposition error (BSSE). Specifically, the intermolecular energy (E_{BSSE}) of DMA-M3 solvents is −6.93 kcal mol^{-1}, which is much

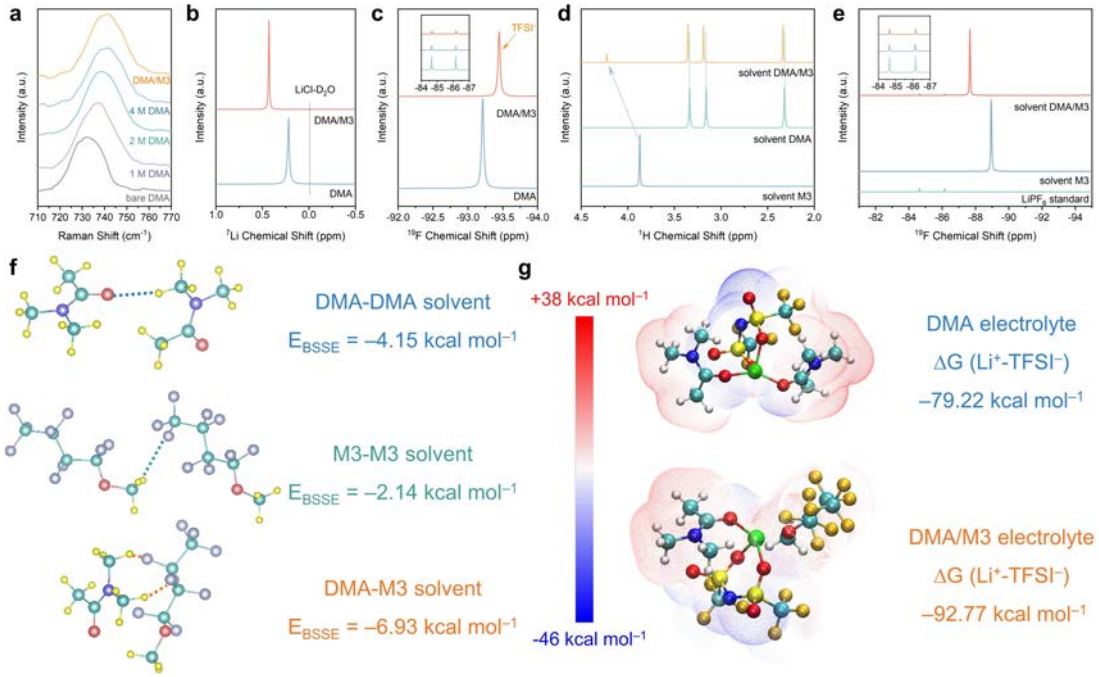

Figure 2. (a) Raman spectra of different electrolytes. (b) ^{7}Li-NMR and (c) ^{19}F-NMR spectra of the DMA and DMA/M3 electrolytes. (d) ^{1}H-NMR and (e) ^{19}F-NMR spectra of the M3, DMA, and DMA/M3 solvents. (f) E_{BSSE} of the DMA-DMA, M3-M3, and DMA-M3 solvents. The color scheme: yellow-H atom, red-O atom, green-C atom, purple-N atom, and blue-F atom. (g) ESP comparison of the DMA and DMA/M3 electrolytes and the binding energy of Li^+-$TFSI^-$ in the electrolytes. The color scheme: grey-H atom, deep yellow-F atom, red-O atom, green-Li atom, blue-N atom, cyan-C atom, and yellow-S atom.

lower than that of DMA-DMA solvents (−4.15 kcal mol^{-1}) and M3-M3 solvents (−2.14 kcal mol^{-1}), demonstrating a preference for heteromolecular interactions in DMA-M3 solvents over homomolecular ones (Figure 2f).

Upon verifying the interaction between the DMA and M3 solvent, density functional theory (DFT) calculations and Ab initio molecular dynamics (AIMD) simulations were conducted to investigate its impact on Li^+ solvation structure. Notably, a longer Li–O bond length was detected in the M3 complex (Figure S10a). Moreover, the binding energy between the Li^+ and M3 diluent (−0.35 eV) is markedly weaker than that of Li^+-DMA (−1.01 eV), indicating that the M3 diluent is unlikely to be incorporated into the Li^+ solvation shells (Figure S10b). AIMD simulations were further conducted to investigate the solvation structures in different electrolytes. Two sharp peaks corresponding to $Li–O_{DMA}$ and $Li–O_{TFSI}$ pairs are identified at 1.85 Å and 1.95 Å for both electrolytes, while one small and wide peak of $Li–O_{M3}$ pair is observed in the DMA/M3 electrolyte, signifying that the M3 molecules are barely coordinated with Li^+ (Figure S11). In particular, a much stronger $Li–O_{TFSI}$ pair is observed in the DMA/M3 electrolyte due to the intermolecular interactions between the DMA and M3 solvent, indicating that the M3 addition augments the interactions of Li^+ with $TFSI^-$. Furthermore, the alteration in the distribution of negative charges on the surface of the solvation clusters of Li^+-DMA/DMA-$TFSI^-$ to Li^+-DMA/M3-$TFSI^-$ also demonstrates the strength of Li^+-$TFSI^-$ coordination. As presented in Figure 2g, the ESP calculations reveal a reduction in negative charge distribution post-M3 addition, indicating that the molecular interaction between the DMA and M3 solvent enhances the binding energy of Li^+-$TFSI^-$ (i.e. −92.77 kcal mol^{-1} vs. −79.22 kcal mol^{-1}). Consequently, both the experiment and calculation results corroborate that the addition of the M3 diluent maintain the benefits of the Li^+ solvation structure in HCE while the interaction between the DMA and M3 solvent induces an increased binding of Li^+-$TFSI^-$.

After confirming the increase involvement of anions in the Li^+ solvation structure within the DMA/M3 electrolyte, the stability of the Li metal anode was investigated via long-term cycling test for Li||Li symmetrical cells. Figure 3a illustrates the cycling performance of Li||Li cells at 0.1 mA cm^{-2} and 0.1 mAh cm^{-2} for each stripping/plating process. The cell with the DMA electrolyte exhibits stable cycling for 760 h, followed by a rapid increment in voltage

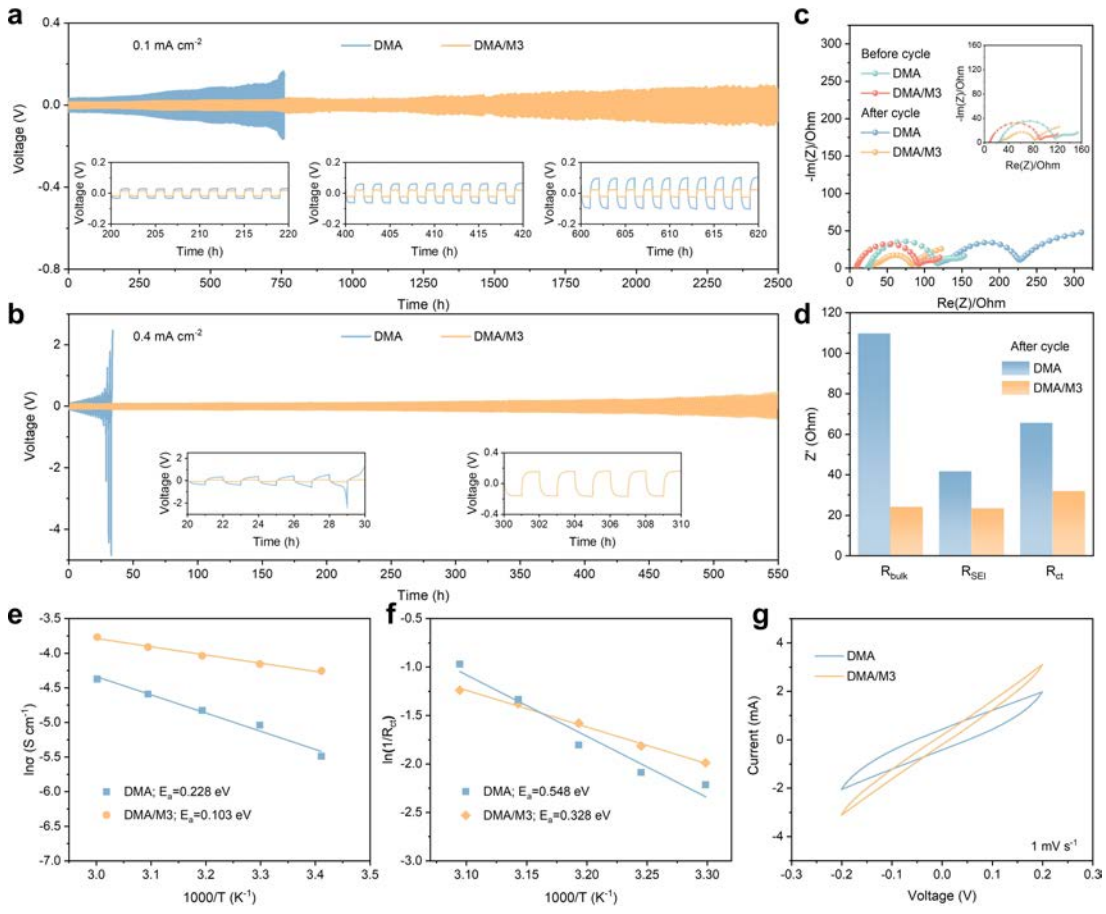

Figure 3. Cycling performance of Li||Li symmetrical cells at (a) 0.1 mA cm^{-2} and (b) 0.4 mA cm^{-2} with each plating/stripping process of 1 h. (c) Nyquist plots of Li||Li cells with different electrolytes before and after cycling. (d) R_{bulk}, R_{SEI}, and R_{ct} of Li||Li cells with different electrolytes after cycling. (e) Arrhenius curves of the DMA and DMA/M3 electrolytes. (f) Arrhenius plots and corresponding E_a from R_{ct} in Li||Li symmetrical cells. (g) CV curves of the Li||Li symmetrical batteries at 1 mV s^{-1}.

polarization. By contrast, in the DMA/M3 electrolyte, the cell could sustain a lower overpotential for an extended cycle life of 2500 h. This trend is also observed at a higher current density of 0.4 mA cm^{-2}. The DMA/M3-based symmetrical batteries continue exhibiting superior electrochemical performance (550 h), whereas the cells with the DMA electrolyte rapidly polarize after only 28 h (Figure 3b). Moreover, the Coulombic efficiency (CE) of Li–Cu cell with the DMA/M3 electrolyte in the O_2 atmosphere could approach nearly 90 % after 50 cycles and is consistently higher than the DMA electrolyte-based cell (Figure S12a, b). Furthermore, the DMA/M3-based Li–Cu cell also has lower Li stripping/plating overpotential than the cell with the DMA electrolyte (Figure S12c, d). Therefore, the introduction of M3 diluent could facilitate the construction of stable SEI films to improve the cyclability of Li anode.

Electrochemical impedance spectroscopy (EIS) of the Li||Li cells was employed to further reveal the stability of the electrode/electrolyte interface. As presented in Figure 3c, due to the high concentration and viscosity of the DMA electrolyte, the impedance of the DMA-based cell is higher than that of the cell with the DMA/M3 electrolyte before cycling. After cycling, a sharp growth in R_{bulk}, R_{SEI}, and R_{ct} is observed in the batteries with the DMA electrolyte (Figure 3d), which could be contributed to the formation of an uneven SEI on the Li metal anode during constant deposition/stripping process. On the contrary, impedance is marginally reduced in the cells with the DMA/M3 electrolyte upon cycling, suggesting the formation of a stable electrode/electrolyte interface. It is beneficial to the long-term upkeep of the cell. To investigate the enhancement of electrochemical performance, the mass transfer and electrode kinetics of the electrolytes were evaluated. As shown in Figure 3e, the activation energy (E_a) corresponding to the Arrhenius equation is employed to illustrate the migration barrier of Li^+ in the electrolyte.[27] The ionic conductivity of the DMA electrolyte consistently falls below that of the DMA/M3 electrolyte across various temperatures (Figure 1b). Therefore, the E_a for the DMA/M3 electrolyte (0.103 eV) is much lower than that of the DMA electrolyte (0.228 eV), signifying a marked improvement in the Li^+ migration process. In addition, the charge transfer barrier in the electrolyte was also estimated by the Arrhenius plots derived from the R_{ct} in Li||Li symmetrical cells, where the Li^+ de-solvation process is the rate-determining step.[28] In comparison to the high concentration DMA electrolyte (0.548 eV), the DMA/M3 electrolyte displays a reduced E_a of 0.328 eV (Figure 3f), indicating a much easier de-solvation process and faster charge transfer kinetics could be obtained in the DMA/M3 electrolyte. Besides, the dynamics of lithium plating and stripping process were assessed through cyclic voltammetry (CV) tests of the Li||Li symmetrical cells. The CV curve of the DMA/M3-based cell shows a steeper slope and higher reduction and oxidation peak current compared to the DMA electrolyte, implying a more facile Li deposition/dissolution reaction (Figure 3g).[29] As a result, the faster ion transport, accelerated mass transfer, and enhanced electrode kinetics in the DMA/M3 electrolyte contribute to the less polarization and prolonged cycle life of the symmetrical batteries.

Subsequently, scanning electron microscopy (SEM) and X-ray photoelectron spectroscopy (XPS) analysis were carried out to detect the Li morphology post-cycling and investigate the interfacial chemistry between Li and the electrolytes in depth. As shown in Figure 4a and 4b, the Li metal anode exhibits an uneven and rough surface in the DMA electrolyte. On the contrary, a quite smooth Li surface devoid of dendrite growth is observed in the DMA/

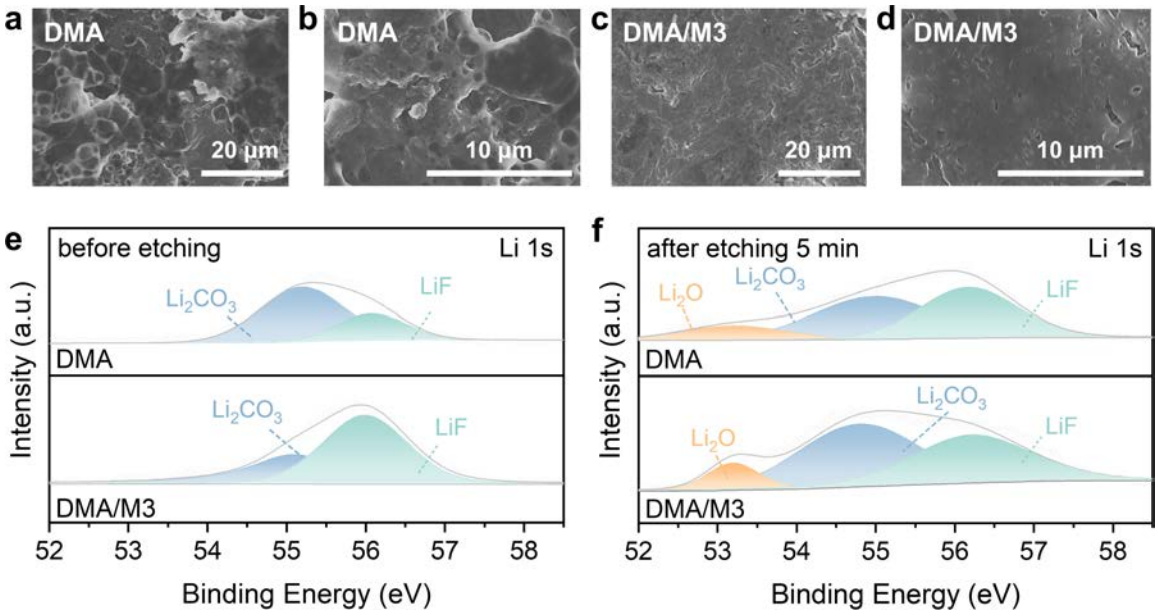

Figure 4. SEM images of the Li anodes after cycling in the (a, b) DMA and (c, d) DMA/M3 electrolytes. Li 1s XPS spectra of the Li anodes in the DMA and DMA/M3 electrolytes (e) before and (f) after etching for 5 min.

M3 electrolyte (Figure 4c, d), demonstrating the uniform deposition behavior of Li and enhanced electrode/electrolyte interface stability. The Li 1s XPS spectra before and after etching are presented in Figure 4e and 4f, respectively. The SEI film in both electrolytes primarily consists of anion-derived inorganic substances, such as LiF and Li_2CO_3. These inorganic constituents are conducive to stabilizing the Li/electrolyte interface.[30,31] Specifically, for the outer-SEI, the Li surface in both electrolytes is predominantly composed of Li_2CO_3 and LiF. Notably, the SEI within the DMA/M3 electrolyte exhibits a significantly higher LiF content compared to the DMA electrolyte (Figure 4e). After etching for 5 min, the presence of Li_2O is observed in the inner SEI. In particular, the Li_2O content in the DMA/M3 electrolyte significantly exceeds that in the DMA electrolyte (Figure 4f, S13). This can be attributed to the fact that the more anions involve in the Li^+ solvation structure of the DMA/M3 electrolyte. As a result, these anions decompose on the Li metal anode and form anion-derived, inorganic-rich SEI. This process facilitates the formation of a more stable SEI film, thereby enhancing the electrode/electrolyte interface and leading to prolonged cycling lives.

Based on the superior compatibility of the DMA/M3 electrolyte with the Li metal anode, coupled with its resistance to attack by oxygen active intermediates such as O_2^- and $^1O_2$, the practical application capability in Li–O_2 batteries was explored. As shown in Figure 5a, the cells with the DMA/M3 electrolyte achieve consistently larger discharge capacities than the cells with the DMA electrolyte at each current density. Specifically, the capacity of Li–O_2 batteries with the DMA/M3 electrolyte could provide 14700, 11094, and 9687 mAh g^{-1} at 300, 500, and 1000 mA g^{-1}, respectively, while the batteries with the DMA electrolyte could only reach 5485, 4201, and 3569 mAh g^{-1} at the same conditions. Furthermore, even though there is no catalyst loading on the cathode, the batteries with both kinds of electrolytes can be fully recharged and maintain a charge platform below the 4.5 V threshold. The enhancement in discharge capacity is attributed to the accelerated mass transfer process triggered by the reduced electrolyte concentration and the presence of C–F bonds in the M3 diluent resulted increase of oxygen solubility in the electrolyte (Figure 1d). SEM and X-ray diffraction (XRD) characterization were further conducted to detect the morphology

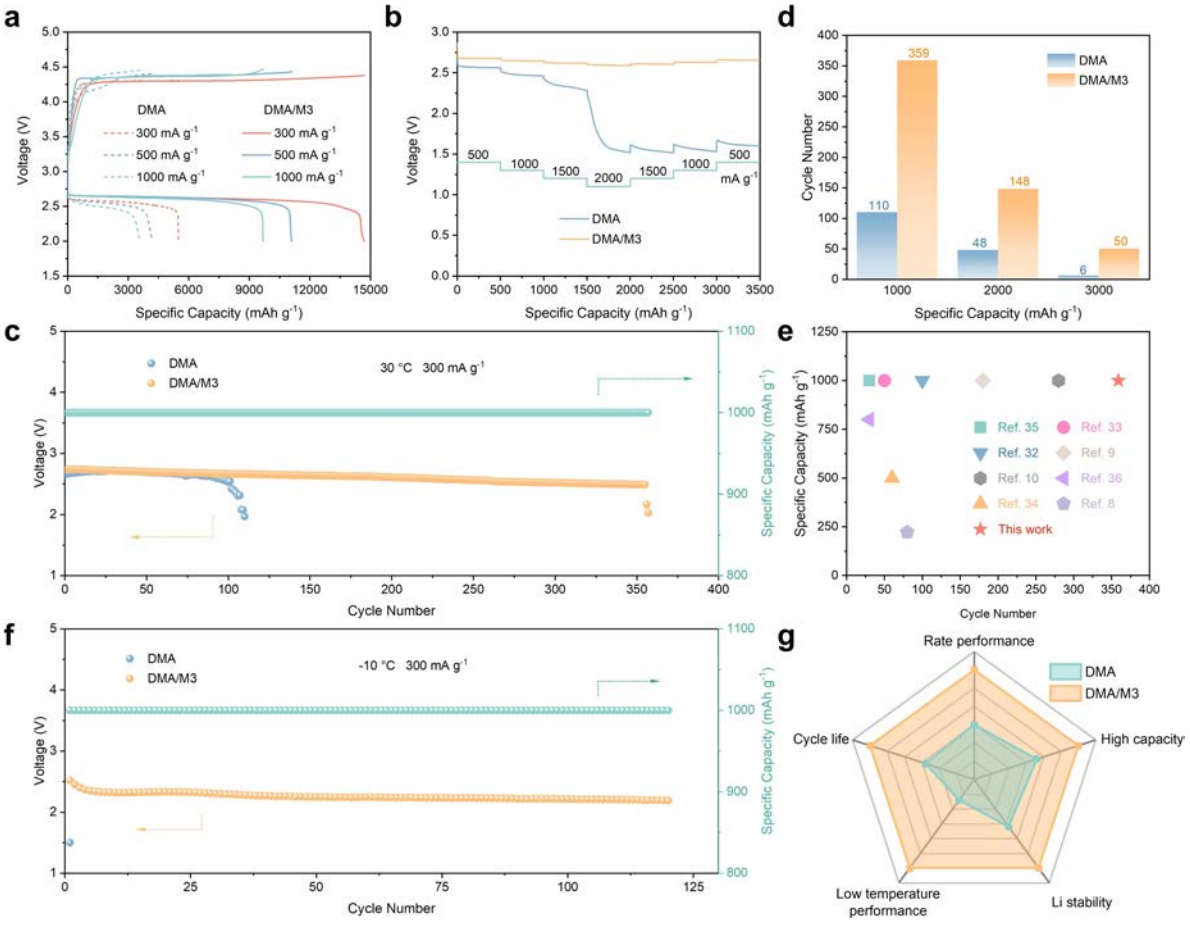

Figure 5. (a) Full discharge-charge curves of Li–O_2 batteries at different current densities. (b) Rate performance of Li–O_2 batteries. (c) Cycling performance of Li–O_2 batteries with a limited capacity of 1000 mAh g^{-1} at 300 mA g^{-1} and 30 °C. (d) Cycle numbers of Li–O_2 batteries with different electrolytes and specific capacites. (e) Comparison of electrochemical performance of amide-based Li–O_2 batteries. (f) Cycling performance of Li–O_2 batteries with a limited capacity of 1000 mAh g^{-1} at 300 mA g^{-1} and −10 °C. (g) Comparison of the performance of Li–O_2 batteries in the DMA and DMA/M3 electrolytes.

and composition of the discharge products. As shown in Figure S14, the SEM image of the discharge products in the DMA/M3 electrolyte exhibits larger particles than that in the DMA electrolyte, consistent with its large discharge capacity. Besides, the XRD patterns in Figure S15 show that the peaks of 32.9°, 35.0°, and 58.7° correspond to Li_2O_2. No peaks of LiOH and Li_2CO_3 are observed on the cathode, implying that the M3 diluent remains stable through the discharge process with no variation of discharge products.

Considering that the introduction of the M3 diluent would not alter the electrochemical reaction in Li–O_2 batteries, the rate performance and cycling performance were further checked. As presented in Figure 5b, at an initial discharge of 500 mA g^{-1}, the cell with the DMA electrolyte displays a lower discharge voltage compared to that with the DMA/M3 electrolyte due to the polarization induced by the high concentration of the electrolyte. In subsequent continuous current density transformations at 500 mA g^{-1} intervals, a significant voltage drop occurred at 2000 mA g^{-1} in the DMA-based cells, and the discharge platform could not be restored as the current density decreased. In contrast, the DMA/M3-based cells still maintain stable discharge curves due to the accelerated mass transfer and improved electrode kinetics. Beyond rate performance, the Li–O_2 batteries with the DMA/M3 electrolyte also exhibit excellent long-cycle performance. The cycling performance of Li–O_2 batteries at 300 mA g^{-1} and 1000 mAh g^{-1} are presented in Figure 5c. In the DMA electrolyte, the batteries could only operate for 110 cycles (Figure S16a) until the terminal voltage dropped to 2.0 V. On the contrary, the cycle performance of the cells with DMA/M3 electrolyte significantly improves to 359 cycles (Figure S16b). At higher capacities of 2000 mA g^{-1} and 3000 mA g^{-1}, the DMA/M3-based battery could still stably operate for 148 (Figure S17) and 50 cycles (Figure S18), respectively, which is significantly higher than that of the DMA electrolyte (Figure 5d). It is worth to mention that the lifetime achieved here is the longest reported in the current amide-based Li–O_2 batteries (Figure 5e).[8–10,32–36]

Subsequently, in situ pressure monitoring test[37] and gas evolution detection of Li–O_2 batteries during discharge and charge processes were conducted to confirm that the cell operation is reliant on the Li_2O_2/O_2 reaction. As presented in Figure S19a, b, the Li–O_2 batteries with both the DMA and DMA/M3 electrolytes undergo nearly a $2e^-$ per O_2 reaction during the discharge process. Moreover, the XRD patterns (Figure S20) and SEM images (Figure S21a, b) of the cathodes after cycling reveal the formation of Li_2O_2. Acid-base titration and iodometric titration were further conducted to evaluate the yield of Li_2O_2 (Figure S22).[38] In the DMA and DMA/M3 electrolyte, the yields of Li_2O_2 are found to be 90.70% and 94.71%, respectively (Table S1, Figure S23). This indicates that Li–O_2 batteries with the DMA/M3 electrolyte undergo less side reactions. During the charge process, in situ pressure monitoring test in Figure S19c, d shows that the Li–O_2 cells based on DMA and DMA/M3 electrolytes exhibit the oxygen evolution reaction of 1.86 e^-/O_2 and 1.93 e^-/O_2, respectively, in which the DMA/M3 could enable the cells to proceed along a nearly two-electron reaction with high reversibility. Differential electrochemical mass spectrometry (DEMS) further reveals that a large amount of O_2 evolution is detected in the cell with the DMA/M3 electrolyte compared to that with the DMA electrolyte (Figure S19e, f). Moreover, the XRD patterns (Figure S20) and SEM image (Figure S21d) of the re-charged cathodes confirm that the Li_2O_2 discharge products of the battery with the DMA/M3 electrolyte can be fully decomposed during the charging process. However, Figure S21c shows that several discharge products still exist after charging in the battery with the DMA electrolyte, which corresponds to the low O_2 evolution amount in Figure S19e. Expect for the cathode side, the SEM characterization of the Li metal anodes after cycling in Li–O_2 batteries was performed to validate the protective effect of M3 diluent on the Li metal anode. As presented in Figure S24, the Li anode cycled in the DMA/M3 electrolyte exhibits a smooth surface with less cracks. On the contrary, in the DMA electrolyte, obvious corrosion and cracks can be observed on the Li surface. Therefore, the addition of M3 diluent shows positive effect on Li anode protection in practical Li–O_2 batteries. Consequently, the Li–O_2 batteries with the DMA/M3 electrolyte exhibit superior re-chargeability and electrochemical stability compared to those with the DMA electrolyte.

In view of the superior electrochemical performance of the DMA/M3-based batteries at normal temperature (30 °C) and the higher ionic conductivity of the electrolyte at low temperature (Figure 1b), the feasibility of the application at low temperature was confirmed. At 0 °C and −10 °C, the Li–O_2 batteries with the DMA/M3 electrolyte exhibit a discharge capacity of 5226 mAh g^{-1} and 3485 mAh g^{-1}, respectively. On the contrary, the cells with the high concentrated DMA electrolyte die quickly at −10 °C (Figure S25). Additionally, the DMA/M3-based cells also display a much improved cycling performance at low temperatures, which could run stably for 143 (Figure S26) and 120 cycles (Figure 5f, S27) at 0 °C and −10 °C, respectively. Therefore, the DMA/M3 electrolyte presents promising applications for $Li-O_2$ batteries in both standard and low temperature conditions. Furthermore, the electrolyte design strategy of introducing an HFE diluent to achieve high-performance Li–O_2 batteries is universally applicable. The electrochemical performance of another HFE, 1,1,2,2-tetrafluoroethyl isobutyl ether (TFEiBE, Figure S28) with less –CH_2– and –CH– functional groups and rich in stable –CH_3 and C–F groups, for Li–O_2 batteries was also checked. Compared with the cells using the DMA electrolyte, the DMA/TFEiBE-based cells also show prolonged cycle lives of 340th and 128th at 1000 mAh g^{-1} and 2000 mAh g^{-1}, respectively (Figure S29). Even at the low temperature of 0 °C and −10 °C, the cells maintained stable operation for cycles of 116th and 80th, respectively (Figure S30). Consequently, the electrolyte regulation strategy not only retains the benefits of high concentration electrolyte but also promotes increased Li^+-anions coordination in the solvation structure due to the intermolecular interactions with the DMA solvent and M3 diluent. The superior compatibility of the DMA/M3 electrolyte with the Li metal anode, coupled with its resistance to attack by oxygen active intermediates,

facilitates the achievement of stable Li–O_2 batteries with high capacity, excellent rate performance, and long cycle lives at both room temperature and low temperatures (Figure 5g).

Conclusion

In summary, we have developed a localized high concentration electrolyte by incorporating an innovative M3 hydrofluoroether diluent to stabilize the Li metal anode within the DMA-based electrolyte. The dilution of M3 not only enhances the fundamental properties of the electrolyte but also bolsters its resilience against attacks from oxygen reduction intermediates due to the stable $–CH_3$ and C–F bonds in the structure. Additionally, the strong electron-withdrawing groups (–F) presented in the M3 diluent facilitate coordination with the electron-donating groups ($–CH_3$) in the DMA solvent. This intermolecular interaction promotes increased Li^+-$TFSI^-$ alignments with the introduction of only a small amount of M3, resulting in an anion-derived inorganic-rich SEI to enhance the stability of the Li anode. The optimization of the DMA/M3 electrolyte leads to improvements in mass transfer, electrode kinetics, and lithium anode stability, culminating in the development of stable and high-performance Li–O_2 batteries (359^{th} at 30 °C, 120^{th} at −10 °C). The significant findings of this study provide a novel guideline to address the incompatibility issue between Li and electrolyte and open up a new avenue for promoting the practical application of alkali metal-air batteries.

Acknowledgements

This work was financially supported by the National Key R&D Program of China (2019YFA0705704), National Natural Science Foundation of China (U23A20575, U22A20437, 52171194, 52271140), CAS Project for Young Scientists in Basic Research (YSBR-058), Youth Innovation Promotion Association CAS (Grant 2020230), and National Natural Science Foundation of China Outstanding Youth Science Foundation of China (Overseas).

Conflict of Interest

The authors declare no conflict of interest.

Data Availability Statement

The data that support the findings of this study are available from the corresponding author upon reasonable request.

Keywords: Li–O_2 battery · Hydrofluoroether · N,N-dimethylacetamide · Solvent-diluent interaction · Anion–derived SEI

[1] Q. K. Zhang, X. Q. Zhang, J. Wan, N. Yao, T. L. Song, J. Xie, L. P. Hou, M. Y. Zhou, X. Chen, B. Q. Li, R. Wen, H. J. Peng, Q. Zhang, J. Q. Huang, *Nat. Energy* **2023**, *8*, 725–735.
[2] Z. Z. Wu, Y. H. Tian, H. Chen, L. G. Wang, S. S. Qian, T. P. Wu, S. Q. Zhang, J. Lu, *Chem. Soc. Rev.* **2022**, *51*, 8045–8101.
[3] M. Li, C. S. Wang, Z. W. Chen, K. Xu, J. Lu, *Chem. Rev.* **2020**, *120*, 6783–6819.
[4] J. N. Lai, Y. Xing, N. Chen, L. Li, F. Wu, R. J. Chen, *Angew. Chem. Int. Ed.* **2020**, *59*, 2974–2997.
[5] S. A. Freunberger, Y. H. Chen, N. E. Drewett, L. J. Hardwick, F. Bardé, P. G. Bruce, *Angew. Chem. Int. Ed.* **2011**, *50*, 8609–8613.
[6] Z. M. Huang, H. P. Zeng, M. L. Xie, X. Lin, Z. M. Huang, Y. Shen, Y. H. Huang, *Angew. Chem. Int. Ed.* **2019**, *58*, 2345–2349.
[7] D. Sharon, M. Afri, M. Noked, A. Garsuch, A. A. Frimer, D. Aurbach, *J. Phys. Chem. Lett.* **2013**, *4*, 3115–3119.
[8] W. Walker, V. Giordani, J. Uddin, V. S. Bryantsev, G. V. Chase, D. Addison, *J. Am. Chem. Soc.* **2013**, *135*, 2076–2079.
[9] Y. Yu, G. Huang, J.-Y. Du, J.-Z. Wang, Y. Wang, Z.-J. Wu, X.-B. Zhang, *Energy Environ. Sci.* **2020**, *13*, 3075–3081.
[10] C. L. Li, G. Huang, Y. Yu, Q. Xiong, J. M. Yan, X. B. Zhang, *J. Am. Chem. Soc.* **2022**, *144*, 5827–5833.
[11] S. R. Chen, J. M. Zheng, L. Yu, X. D. Ren, M. H. Engelhard, C. J. Niu, H. Lee, W. Xu, J. Xiao, J. Liu, J. G. Zhang, *Joule* **2018**, *2*, 1548–1558.
[12] X. L. Fan, X. Ji, L. Chen, J. Chen, T. Deng, F. D. Han, J. Yue, N. Piao, R. X. Wang, X. Q. Zhou, X. Z. Xiao, L. X. Chen, C. S. Wang, *Nat. Energy* **2019**, *4*, 882–890.
[13] X. D. Ren, S. R. Chen, H. Lee, D. H. Mei, M. H. Engelhard, S. D. Burton, W. G. Zhao, J. M. Zheng, Q. Y. Li, M. S. Ding, M. Schroeder, J. Alvarado, K. Xu, Y. S. Meng, J. Liu, J. G. Zhang, W. Xu, *Chem* **2018**, *4*, 1877–1892.
[14] C. M. Efaw, Q. Wu, N. Gao, Y. Zhang, H. Zhu, K. Gering, M. F. Hurley, H. Xiong, E. Hu, X. Cao, W. Xu, J.-G. Zhang, E. J. Dufek, J. Xiao, X.-Q. Yang, J. Liu, Y. Qi, B. Li, *Nat. Mater.* **2023**, *22*, 1531–1539.
[15] X. Yang, B. Zhang, Y. Tian, Y. Wang, Z. Q. Fu, D. Zhou, H. Liu, F. Y. Kang, B. H. Li, C. S. Wang, G. X. Wang, *Nat. Commun.* **2023**, *14*, 925.
[16] X. D. Ren, L. F. Zou, X. Cao, M. H. Engelhard, W. Liu, S. D. Burton, H. Lee, C. J. Niu, B. E. Matthews, Z. H. Zhu, C. M. Wang, B. W. Arey, J. Xiao, J. Liu, J. G. Zhang, W. Xu, *Joule* **2019**, *3*, 1662–1676.
[17] W. J. Kwak, H. S. Lim, P. Gao, R. Feng, S. Chae, L. Zhong, J. Read, M. H. Engelhard, W. Xu, J. G. Zhang, *Adv. Funct. Mater.* **2020**, *31*, 2002927.
[18] H. H. Liang, Z. Ma, Y. Q. Wang, F. Zhao, Z. Cao, L. Cavallo, Q. Li, J. Ming, *ACS Nano* **2023**, *17*, 18062–18073.
[19] A. Sagadevan, K. C. Hwang, M. D. Su, *Nat. Commun.* **2017**, *8*, 1812.
[20] Y. G. Zou, Z. Ma, G. Liu, Q. Li, D. M. Yin, X. J. Shi, Z. Cao, Z. N. Tian, H. Kim, Y. J. Guo, C. S. Sun, L. Cavallo, L. M. Wang, H. N. Alshareef, Y. K. Sun, J. Ming, *Angew. Chem. Int. Ed.* **2023**, *62*, e202216189.
[21] Q. Zhao, Y. H. Zhang, G. R. Sun, L. N. Cong, L. Q. Sun, H. M. Xie, J. Liu, *ACS Appl. Mater. Interfaces* **2018**, *10*, 26312–26319.
[22] S. A. Freunberger, Y. H. Chen, Z. Q. Peng, J. M. Griffin, L. J. Hardwick, F. Bardé, P. Novák, P. G. Bruce, *J. Am. Chem. Soc.* **2011**, *133*, 8040–8047.
[23] W.-J. Kwak, S. Chae, R. Feng, P. Gao, J. Read, M. H. Engelhard, L. Zhong, W. Xu, J.-G. Zhang, *ACS Energy Lett.* **2020**, *5*, 2182–2190.
[24] W. J. Kwak, H. Kim, Y. K. Petit, C. Leypold, T. T. Nguyen, N. Mahne, P. Redfern, L. A. Curtiss, H. G. Jung, S. M. Borisov, S. A. Freunberger, Y. K. Sun, *Nat. Commun.* **2019**, *10*, 1380.

[25] Y. Umebayashi, K. Matsumoto, M. Watanabe, K. Katoh, S.-i. Ishiguro, *Anal. Sci.* **2001**, *17*, 323–326.
[26] L. Wang, K. Uosaki, H. Noguchi, *J. Phys. Chem. C* **2020**, *124*, 12381–12389.
[27] X. Zhang, S. Wang, C. J. Xue, C. Z. Xin, Y. H. Lin, Y. Shen, L. L. Li, C. W. Nan, *Adv. Mater.* **2019**, *31*, e1806082.
[28] C. X. Chu, N. N. Wang, L. L. Li, L. D. Lin, F. Tian, Y. L. Li, J. Yang, S. X. Dou, Y. T. Qian, *Energy Storage Mater.* **2019**, *23*, 137–143.
[29] J. Lopez, A. Pei, J. Y. Oh, G. J. N. Wang, Y. Cui, Z. A. Bao, *J. Am. Chem. Soc.* **2018**, *140*, 11735–11744.
[30] L. L. Jiang, C. Yan, Y. X. Yao, W. Cai, J. Q. Huang, Q. Zhang, *Angew. Chem. Int. Ed.* **2020**, *60*, 3402–3406.
[31] X. Q. Zhang, T. Li, B. Q. Li, R. Zhang, P. Shi, C. Yan, J. Q. Huang, Q. Zhang, *Angew. Chem. Int. Ed.* **2020**, *59*, 3252–3257.
[32] E. J. Yoo, H. S. Zhou, *ACS Appl. Mater. Interfaces* **2020**, *12*, 18490–18495.
[33] Y. Kim, D. Koo, S. Ha, S. C. Jun, T. Yim, H. Kim, S. K. Oh, D. M. Kim, A. Choi, Y. Kang, K. H. Ryu, M. Jang, Y. K. Han, S. M. Oh, K. T. Lee, *ACS Nano* **2018**, *12*, 4419–4430.
[34] H. D. Lim, Y. S. Yun, Y. Ko, Y. Bae, M. Y. Song, H. J. Yoon, K. Kang, H. J. Jin, *Carbon* **2017**, *118*, 114–119.
[35] F. Lepoivre, A. Grimaud, D. Larcher, J.-M. Tarascon, *J. Electrochem. Soc.* **2016**, *163*, A923–A929.
[36] S. Choudhury, C. T. C. Wan, W. I. Al Sadat, Z. Y. Tu, S. Lau, M. J. Zachman, L. F. Kourkoutis, L. A. Archer, *Sci. Adv.* **2017**, *3*, e1602809.
[37] K. Chen, G. Huang, J. L. Ma, J. Wang, D. Y. Yang, X. Y. Yang, Y. Yu, X. B. Zhang, *Angew. Chem. Int. Ed.* **2020**, *59*, 16661–16667.
[38] Y. Qiao, S. C. Wu, J. Yi, Y. Sun, S. H. Guo, S. X. Yang, P. He, H. S. Zhou, *Angew. Chem. Int. Ed.* **2017**, *56*, 4960–4964.

Manuscript received: February 18, 2024
Accepted manuscript online: July 18, 2024
Version of record online: ■■, ■■

Research Article

Lithium Oxygen Batteries

D.-Y. Yang, J.-Y. Du, Y. Yu, Y.-Q. Fan, G. Huang, X.-B. Zhang,* H.-J. Zhang* **e202403432**

Stable Lithium Oxygen Batteries Enabled by Solvent-diluent Interaction in N,N-dimethylacetamide-based Electrolytes

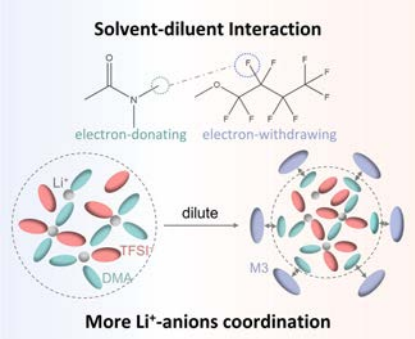

A rationally selected methyl nonafluorobutyl ether (M3) diluent is introduced into the N,N-dimethylacetamide (DMA)-based electrolyte to construct a localized high concentration electrolyte. The interaction between the DMA solvent and M3 diluent increases the coordination number of Li^+-anions, facilitating the formation of an anion-derived inorganic-rich solid electrolyte interphase to improve the Li metal stability and consequently realizing stable and high-performance Li–O_2 batteries.